Molecular Therapy
Nucleic Acids
Original Article

circCYFIP2 Acts as a Sponge of miR-1205 and Affects the Expression of Its Target Gene E2F1 to Regulate Gastric Cancer Metastasis

Jing Lin,[1] Shasha Liao,[2] E. Li,[2] Zewa Liu,[1] Ruihua Zheng,[1] Xiaohua Wu,[2] and Wanting Zeng[3]

[1]The First Affiliated Hospital of Shantou University Medical College, Shantou 515041, China; [2]The First Affiliated Hospital of Shantou University Medical College, Longhu People's Hospital Shantou, Shantou 515041, China; [3]University College, London, UK

Accumulating evidence suggested that circular RNAs (circRNAs) play critical roles in the initiation and progression of malignant cancers. However, the roles of circRNAs in gastric cancer (GC) remain largely unknown. In the present study, we investigated the expression of circRNAs in 5 GC tissues with metastasis and 5 GC tissues without metastasis by microarray analysis. We focused on hsa_circ_0003506, which was spliced from CYFIP2 gene located at chr5:156786012–156788606 and finally formed a sense-overlapping circular transcript of 366 nt, and thus we named it circCYFIP2. circCYFIP2 was found to be significantly upregulated in GC tissues and cell lines. High expression of circCYFIP2 was associated with metastasis and poor prognosis of GC patients. Function assays revealed that overexpression or knockdown of circCYFIP2 significantly enhanced or reduced GC cell proliferation and invasion abilities. In mechanism, we found that circCYFIP2 might serve as a competing endogenous RNA (ceRNA) of microRNA-1205 (miR-1205) in GC progression. Besides, E2F1 was found to be a target of miR-1205. Collectively, our findings suggested that circCYFIP2 might serve as an oncogenic circRNA to promote GC progression via the miR-1205/E2F1 axis, which provided a potential therapeutic target for the treatment of GC.

INTRODUCTION

Gastric cancer (GC) is responsible for a notable proportion of cancer morbidity and mortality worldwide.[1] Although many mechanisms underlying the onset and progression of GC have been revealed over the past few years, delayed diagnosis and treatment are largely responsible for the high mortality rate among GC patients.[2] Because there are limited therapeutic approaches for treating advanced GC, it is urgent that we search for novel biomarkers and prognostic indicators to reflect the disease status and develop more therapeutic targets for this lethal disease.[3]

Circular RNAs (circRNAs), a category of noncoding RNAs (ncRNAs), play a crucial role in the process of transcriptional and posttranscriptional gene expression.[4] A large number of research studies have revealed that circRNAs perform critical functions in various physiological or pathological processes.[5] circRNAs mediate gene expression by sponging microRNAs (miRNAs) or interacting with other molecules and then inhibit their function.[6] miRNAs are a large class of short (~22 nt) ncRNAs that posttranscriptionally regulate gene expression through direct base pairing to target sites within mRNAs.[7] circRNAs can affect miRNA activities by competing for miRNA-binding sites.[8] However, the function of circRNAs as miRNA sponges has not been clearly elucidated in GC progression.

In this study, we aimed to investigate the role of circRNA in GC metastasis. We collected metastatic and non-metastatic GC tissues and analyzed their circRNA expression patterns. A novel circRNA circCYFIP2 was selected for further study. We assessed the relationship between circCYFIP2 expression and its diagnostic power and clinical significance in GC. Additionally, we investigated the role and underlying mechanism of circCYFIP2 in GC metastasis. Our findings highlight the important role of circCYFIP2-miR-1205-E2F1 axis in GC metastasis and its potential as a therapeutic target for GC.

RESULTS

circCYFIP2 Is Upregulated in GC Tissues and Correlates with the Progression and Poor Prognosis

To characterize metastasis-related circRNA transcripts, we conducted circRNA microarray analysis between 5 GC tissues with metastasis and 5 GC tissues without metastasis. We found a total of 863 differentially expressed circRNAs with a cut-off criteria of fold change >2.0 and $p < 0.05$, of which 487 were upregulated and 376 were downregulated in GC tissues with metastasis. The heatmap showed top 10 dysregulated circRNAs between GC tissues with metastasis and GC tissues without metastasis (Figure 1A). Expression levels of 10 circRNAs selected from the top 10 dysregulated circRNAs were measured by quantitative real-time polymerase chain reaction in GC tissues with metastasis and GC tissues without metastasis (Figure 1B). Among the 863 differentially expressed circRNAs, 329,

Received 25 February 2020; accepted 8 May 2020;
https://doi.org/10.1016/j.omtn.2020.05.007.

Correspondence: Jing Lin, The First Affiliate Hospital, School of Medicine, Shantou University, Shantou 515041, China.
E-mail: drdingwei66@163.com

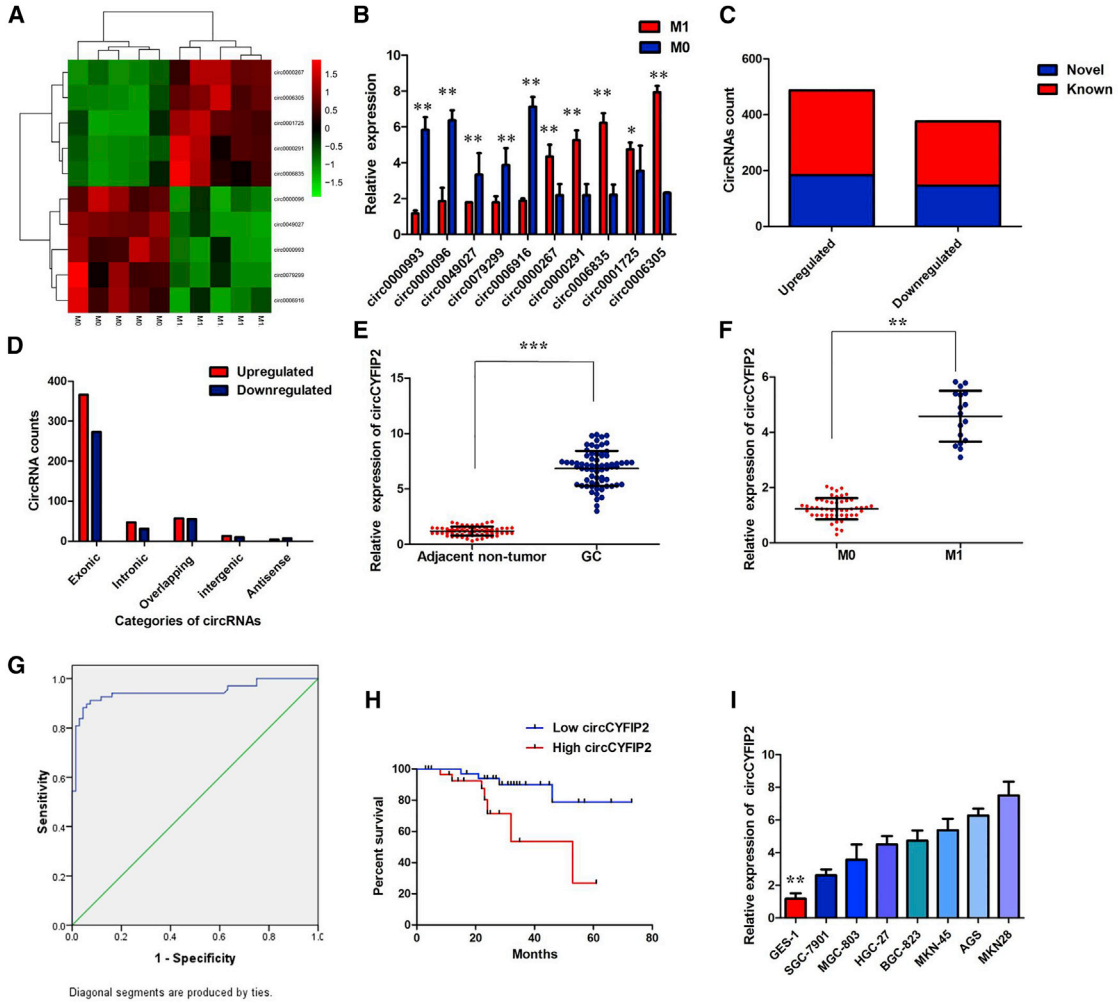

Figure 1. circCYFIP2 Is Upregulated in GC Tissues and Correlates with the Progression and Poor Prognosis

(A) The heatmap showed top 10 dysregulated circRNAs between GC tissues with metastasis and GC tissues without metastasis. (B) Expression levels of top 10 dysregulated circRNAs were measured by quantitative real-time PCR in GC tissues with metastasis and GC tissues without metastasis. (C) Among the 863 differentially expressed circRNAs, 329 circRNAs were verified as novel circRNAs; 534 circRNAs were identified beforehand and listed in the circRNA database. (D) The number of upregulated (red) and downregulated (green) circRNAs according to their categories of formation mode. (E) The level of circCYFIP2 was significantly increased in GC tissues compared to adjacent normal tissues. (F) The level of circCYFIP2 was higher in GC tissues with M1 stage than these with M0 stage. (G) Evaluation the diagnostic performance of circCYFIP2 for GC diagnosis. (H) Kaplan-Meier curve revealed that high expression of circCYFIP2 was relative to a poor overall survival in GC patients. (I) The levels of circCYFIP2 was significantly increased in GC cell lines compared to GES-1 cell; all tests were at least performed three times. Data were expressed as mean ± SD. ***$p < 0.001$; **$p < 0.01$.

including 183 upregulated ones and 146 downregulated ones, were verified as novel circRNAs; 534 circRNAs, including 304 upregulated and 230 downregulated ones, had been identified beforehand and listed in the circRNA database (circBase, http://www.circbase.org; Figure 1C). The 863 identified circRNAs were divided into five different categories on the basis of the way they were produced. Exonic circRNAs consisting of the protein-encoding exons accounted for 74.04% (639/863), intronic circRNAs from intron lariats comprised 9.04% (78/863), sense overlapping circRNAs that originated from exon and other sequence circRNAs comprised 12.98% (112/863), and intergenic circRNAs composed of unannotated sequences of the gene and antisense circRNAs originating from antisense regions equally comprised 3.94% (34/863; Figure 1D). In the top 10 upregulated circRNAs, we found that circCYFIP2, also named hsa_circ_0003506 according to the annotation of circBase (http://www.circbase.org/), was the highest upregulated circRNA in GC tissues with metastasis, which was spliced from CYFIP2 gene located at chr5:156786012–156788606 and finally formed a sense-overlapping circular transcript of 366 nt.

To determine the level of circCYFIP2, we collected 68 pairs of fresh frozen GC tissues and matched normal tissues. The quantitative real-time PCR results showed that consistent with the results of GC cells, circCYFIP2 expression was higher in GC tissues than in normal

Table 1. Association of circCYFIP2 Expression with Clinicopathological Features of HCC Patients

Characteristics	circCYFIP2 -21590444500Low (n = 34)	Expression High (n = 34)	p
Age (years)			
<60	24	20	0.446
≥60	10	14	
Gender			
Female	16	13	0.624
Male	18	21	
Differentiation			
Well	14	9	0.305
Moderate + poor	20	25	
T stage			
T1 + T2	25	13	0.006
T3 + T4	9	21	
N stage			
N0+ N1	17	5	0.003
N2+ N3	17	29	
M stage			
M0	32	24	0.023
M1	2	10	
UICC stage			
I	26	13	0.002
II + III	8	21	
Nerve invasion			
Yes	12	16	0.460
No	22	18	
Vessel invasion			
Yes	11	14	0.615
No	23	20	

gastric tissues (Figure 1E). To further analyze the correlation between the level of circCYFIP2 with clinicopathological features and prognosis, we divided these samples into two groups, high circCYFIP2 group and low circCYFIP2 group, based on the median expression of circCYFIP2. As shown in Table 1, high level of circCYFIP2 was positively correlated with Union for International Cancer Control (UICC) stages, pathological T stages, lymphatic metastasis, distant metastasis, and grades. Also, the level of circCYFIP2 was higher in tissues with M1 stage than these with M0 stage (Figure 1F), suggesting that circCYFIP2 is an oncogenic and metastasis-related circRNA. We used the ROC curve to examine the diagnostic value of circCYFIP2 in GC tissues compared with normal gastric tissues and found the area under the ROC curve (AUC) to be 0.947 (95% CI = 0.905–0.988, $p < 0.0001$; Figure 1G). Furthermore, the Kaplan-Meier analysis showed that GC patients with high circCYFIP2 expression had the significantly poorer overall survival (OS) compared with patients with low circCYFIP2 expression (Figure 1H, $p = 0.0159$). In summary, circCYFIP2 was confirmed to be an appropriate diagnostic and prognostic marker for GC. To detect the level of circCYFIP2 and CYFIP2, we designed two sets of primers, divergent primers that were expected to amplify circCYFIP2 and convergent primers to amplify linear CYFIP2 mRNA. We found that the level of circCYFIP2 was obviously higher in multiple GC cells than in GES-1 cell (Figure 1I). Among these cell lines, MKN-28 cells exhibited the highest level of circCYFIP2, while SGC-7901 cells the lowest level.

To confirm the stability of circCYFIP2, we treated MKN-28 and SGC-7901 cells with RNase R, a processive 3′ to 5′ exoribonuclease. As shown in Figure 2A, circCYFIP2 resisted the digestion of RNase R, but the linear form of CYFIP2 was digested sharply. Moreover, we used Actinomycin D to suppress transcription and measure the half-life of circCYFIP2 in MKN-28 and SGC-7901 cells; we found that circCYFIP2 was more stable than CYFIP2 mRNA (Figure 2B; Figure S1A). In addition, the results of nuclear cytoplasmic fractionation illustrated that circCYFIP2 was predominantly localized in the cytoplasm of MKN-28 and SGC-7901 cells (Figure 2C; Figure S1B), indicating that circCYFIP2 is highly stable in cytoplasm of GC cells.

circCYFIP2 Promotes Proliferation of GC Cells *In Vitro*

To test the functions of circCYFIP2 in GC cells, we designed three small interfering RNAs (siRNAs) that targeted the junction sites of circCYFIP2 and overexpression plasmids of circCYFIP2 and transfected them into MKN-28 and SGC-7901 cells, respectively. circCYFIP2 expression was significantly silenced by si-circ-1, si-circ-2, and si-circ-3, while CYFIP2 mRNA did not change (Figure 2D). Similarly, circCYFIP2 was obviously overexpressed, and no significant change in CYFIP2 mRNA was observed (Figure 2E). Among the three siRNAs, si-circ-1 had the highest knockdown efficiency in MKN-28 cells, so we chose the si-circ-1 in the following experiments. Inhibition of circCYFIP2 reduced the viability of MKN-28 cells (Figure 2F), whereas overexpression of circCYFIP2 promoted the proliferative ability of SGC-7901 cells (Figure 2G). In addition, knockdown of circCYFIP2 significantly decreased the number of cell colonies of MKN-28 cells (Figure 2H) and promoted apoptosis (Figure 2I), whereas ectopic expression of circCYFIP2 in SGC-7901 cells led to an opposite result.

circCYFIP2 Enhances the Growth of Xenograft Tumors of GC Cells *In Vivo*

To investigate the functions of circCYFIP2 *in vivo*, we constructed the stable MKN-28 cells with sh-circCYFIP2 or sh-NC and SGC-7901 cells with circCYFIP2 or NC. The xenograft mouse model was established by subcutaneously injecting of GC cells. After 30 days, all mice were sacrificed and tumor samples were harvested. The volume (Figure 3A) and weight (Figure 3B) of tumors with knockdown of circCYFIP2 were markedly lower than those with control in MKN-28 cells, while the volume (Figure 3D) and weight (Figure 3E) of tumors with overexpression of circCYFIP2 were significantly higher than the control tumors of SGC-7901 cells. After harvesting the subcutaneous tumor tissues, immunohistochemistry (IHC) was performed. Results of

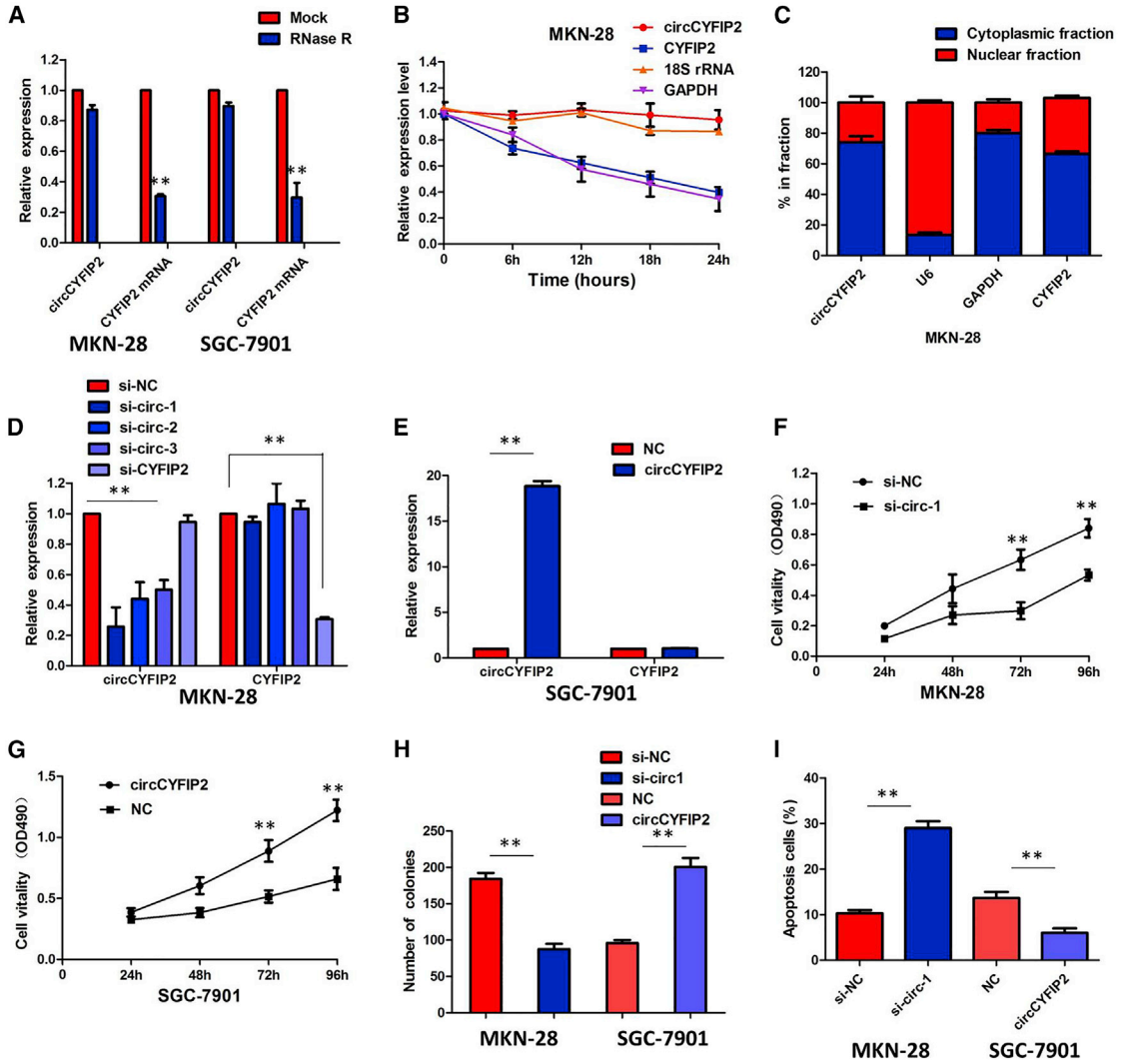

Figure 2. circCYFIP2 Loss of Function Dramatically Impairs the GC Cell Malignant Phenotypes *In Vitro*

(A) Quantitative real-time PCR for the expression of circCYFIP2 and CYFIP2 mRNA in MKN-28 and SGC-7901 cells treated with or without RNase R. (B) Quantitative real-time PCR for the abundance of circCYFIP2 and CYFIP2 in MKN-28 cells treated with Actinomycin D at the indicated time point. (C) Levels of circCYFIP2 in the nuclear and cytoplasmic fractions of MKN-28 cells. (D) The expression of circCYFIP2 was only downregulated by si-circCYFIP2 but was not affected by si-CYFIP2. (E) The circCYFIP2 expression vector markedly increased the expression of circCYFIP2 compared with the empty vector. (F) CCK-8 assays showed circCYFIP2 knockdown significantly decreased the cell viability of MKN-28 cells. (G) Overexpression of circCYFIP2 promoted the proliferative ability of SGC-7901 cells. (H) Colony formation assays revealed that circCYFIP2 affected the numbers of visible colonies of MKN-28 and SGC-7901 cells. (I) Flow cytometry assays revealed that circCYFIP2 affected cell apoptosis of MKN-28 and SGC-7901 cells; all tests were at least performed three times. Data were expressed as mean ± SD. ***$p < 0.001$; **$p < 0.01$.

IHC revealed that xenograft tumors derived from MKN-28 cells with circCYFIP2 knockdown had lower expression of Ki67 (Figure 3C), while the xenograft tumors derived from SGC-7901 cells with overexpression of circCYFIP2 had higher expression of Ki67 than the control group (Figure 3F). Taken together, these findings suggest that circCYFIP2 may play an oncogenic role in GC *in vivo*.

circCYFIP2 Promotes Migration and Invasion of GC Cells *In Vitro*

The mobility of GC cells was prominently decreased by downregulation of circCYFIP2, and the effect was also confirmed by the transwell migration and invasion assays in MKN-28 cells (Figures 4A and 4B). Nevertheless, overexpression of circCYFIP2 promoted the migration and invasion of SGC-7901 cells (Figures 4C and 4D). Taken together, these findings suggest that circCYFIP2 promotes the migration and invasion of GC *in vitro*.

circCYFIP2 Acted as miR-1205 Sponge in GC Cells

According to the hypothesis of competing endogenous RNA (ceRNA), circRNAs may promote the expression of target genes by sponging miRNAs. Since circCYFIP2 is located in the cytoplasm and exhibits high

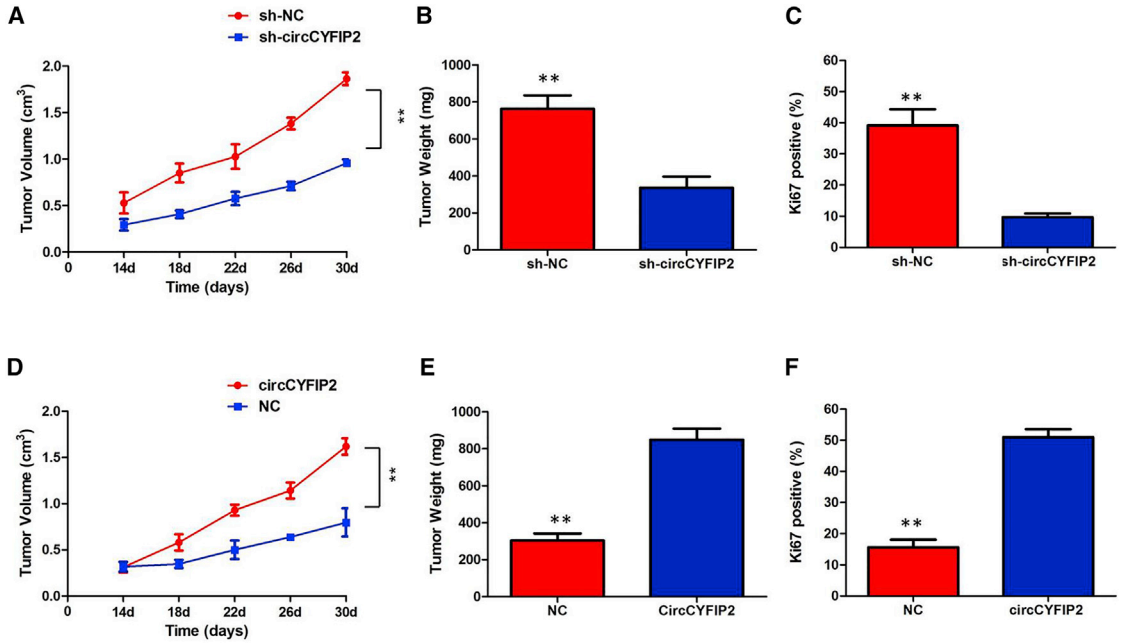

Figure 3. circCYFIP2 Enhances the Growth of Xenograft Tumors of GC Cells *In Vivo*

(A) The volume of subcutaneous xenograft tumors of MKN-28 cells isolated from nude mice. (B) The weight of subcutaneous xenograft tumors of MKN-28 cells isolated from nude mice. (C) IHC analysis was performed to examine the expression levels of KI67 in xenograft tumors of MKN-28 cells isolated from nude mice. (D) The volume of subcutaneous xenograft tumors of SGC-7901 cells isolated from nude mice. (E) The weight of subcutaneous xenograft tumors of SGC-7901 cells isolated from nude mice. (F) IHC analysis was performed to examine the expression levels of KI67 in xenograft tumors of SGC-7901 cells isolated from nude mice. Data were expressed as mean ± SD. ***$p < 0.001$; **$p < 0.01$.

stability, we speculated that circCYFIP2 could act as a miRNA sponge to increase target gene expression. We therefore analyzed the sequence of circCYFIP2 using miRanda, PITA, and RNAhybrid and identified five candidate miRNAs by overlapping the prediction results of the miRNA recognition elements in the circCYFIP2 sequence (miRNA-1205, miRNA-1184, miRNA-1827, miRNA-1256, and miRNA-1243; Figure 5A). It is well known that miRNAs usually silence gene expression by combining with the AGO2 protein and form the RNA-induced silencing complex (RISC). In the context of ceRNA mechanism, it might be a prevalent phenomenon that AGO2 could bind with both circRNAs and miRNAs. We therefore conducted an RNA immunoprecipitation (RIP) assay to pull down RNA transcripts that bind to AGO2 in MKN-28 and SGC-7901 cells. Indeed, endogenous circCYFIP2 was efficiently pulled down by anti-Ago2 (Figure 5B). To further detect whether circCYFIP2 could sponge miRNAs, we performed a miRNA pull-down assay using biotin-coupled miRNA mimics (miRNA-1205, miRNA-1184, miRNA-1827, miRNA-1256, and miRNA-1243). Interestingly, circCYFIP2 was only efficiently enriched by miR-1205, but not by the other four miRNAs (Figure 5C). To validate the interaction between circCYFIP2 and miR-1205, we obtained the binding sequence between miR-1205 and circCYFIP2 (Figure 5D) and conducted luciferase activity analysis. A subsequent luciferase reporter assay revealed that the luciferase intensity was reduced after the cotransfection of the wild-type (WT) luciferase reporter and miR-1205 mimics, while the mutated luciferase reporter exerted no such effect (Figure 5E, $p < 0.01$). In addition, RIP assay revealed that miR-1205 was efficiently pulled down by the anti-AGO2 antibody but not by the nonspecific anti-immunoglobulin G (IgG) antibody (Figure 5F). Furthermore, silencing of circCYFIP2 did not affect the expression of miR-1205, and transfection of miR-1205 mimics did not affect the expression of circCYFIP2 (Figures 5G and 5H), which indicated circCYFIP2 functions as a miRNA sponge without affecting the expression of sponged miRNAs.

E2F1 Is a Direct Target of miR-1205

To validate whether circCYFIP2 sponges miR-1205 and liberates the expression of its downstream target, we identified five target genes of miR-1205 by overlapping the prediction results of the four algorithms (miRanda, RNAhybrid, miRWalk, and TargetScan) prediction, and miR-1205 could target the 3′ UTRs of CRKL, MTA1, S100A8, E2F1, and BATF3 (Figure 6A). To further verify the downstream targets of circCYFIP2, we detected mRNA levels of 5 candidate target genes after silencing circCYFIP2, and we found that only E2F1 was downregulated (Figure 6B). To verify whether E2F1 was the direct target of miR-1205, we first performed the miRNA biotin pull-down assay. We found that miR-1205 could significantly enrich the 3′ UTR of E2F1 mRNA (Figure 6C). To verify whether the 3′ UTR of E2F1 mRNA was a target of miR-1205 in GC cells, we used a luciferase reporter gene assay. The WT 3′ UTR sequence or mutant (MUT) 3′ UTR sequence of E2F1 was cloned into a luciferase reporter vector. The luciferase activity was significantly inhibited by the miR-

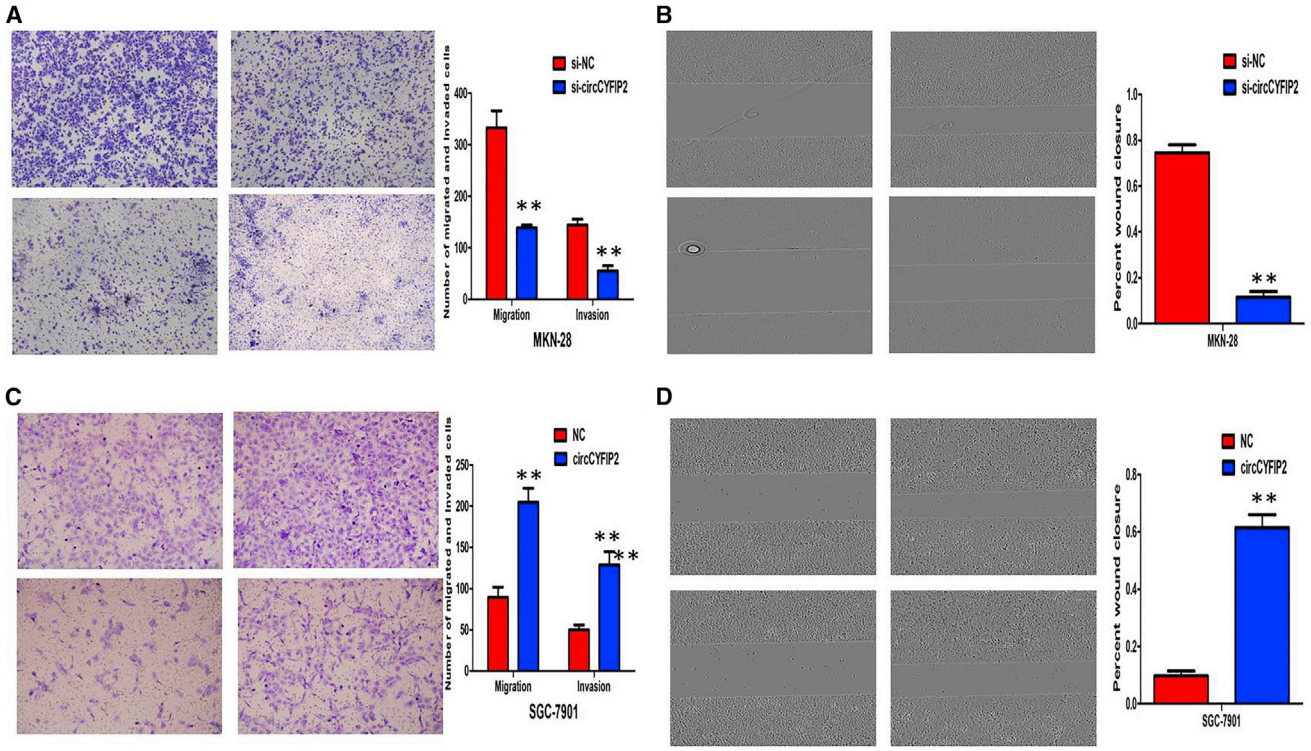

Figure 4. circCYFIP2 Promotes Migration and Invasion of GC Cells *In Vitro*

(A) Transwell migration and invasion assays revealed that circCYFIP2 knockdown greatly inhibited the migration and invasion of MKN-28 cells. (B) Scratch assay revealed that circCYFIP2 knockdown greatly inhibited the migration of MKN-28 cells. (C) Transwell migration and invasion assays revealed that overexpression of circCYFIP2 greatly promoted the migration and invasion of SGC-7901 cells. (D) Scratch assay revealed that overexpression of circCYFIP2 promoted the migration of SGC-7901 cells. Data were expressed as mean ± SD. ***p < 0.001; **p < 0.01.

1205 mimics in WT 3′ UTR sequence-transfected cells. Conversely, the luciferase activity was not inhibited by the miR-1205 mimics in MUT 3′ UTR sequence-transfected cells (Figures 6D and 6E). These results suggested that miR-1205 bind to the 3′ UTR of E2F1 and directly downregulate E2F1 expression.

circCYFIP2 Promotes Cell Proliferation via the circCYFIP2-miR-1205-E2F1 Axis

To validate whether circCYFIP2 promotes cell proliferation via the circCYFIP2-miR-1205-E2F1 axis, we first confirmed that silencing circCYFIP2 decreased the mRNA and protein levels of E2F1 (Figures 7A and 7B), whereas overexpressing circCYFIP2 increased the mRNA and protein levels of E2F1 (Figures 7C and 7D). Then, we designed rescue experiments using miRNA-1205 inhibitors and mimics. At the protein level, miR-1205 partially reversed the effects of circCYFIP2 on E2F1 in GC cell (Figures 7A–7D). More importantly, as revealed by Cell Counting Kit-8 (CCK-8) assays, the miR-1205 mimics could partially rescue the proliferation-promoting effect induced by circCYFIP2 (Figure 7E). To determine the expression levels of E2F1 in GC, we analyzed the GC dataset from the The Cancer Genome Atlas (TCGA) database and found that the level of E2F1 was significantly upregulated in GC tissue compared with normal tissue (Figure 7F). However, Kaplan-Meier survival analysis from TCGA GC datasets suggested that high E2F1 expression in GC tissues is not significantly associated with OS (log-rank test, p = 0.25, Figure 7G) and disease-free survival (DFS; log-rank test, p = 0.22, Figure 7H). All of these data made us draw a conclusion that circCYFIP2 positively regulated E2F1 expression by interacting with miR-1205 in GC cells.

DISCUSSION

In this study, we investigated the expression profiles of circRNAs from 5 GC tissues with metastasis and 5 GC tissues without metastasis by microarray and focused on the expression level of circCYFIP2 in GC, and then elucidated the oncogenic role of circCYFIP2 and explored the underlying mechanism. Our study validated that circCYFIP2 can be considered as a promising biomarker for the diagnosis of GC. The expression of circCYFIP2 was remarkably higher in GC tissues and cell lines, and its upregulation was positively correlated with UICC stages, pathological T stages, lymphatic metastasis, distant metastasis, and grades in GC. Furthermore, we explored the function of circCYFIP2 in GC cells and found that overexpression or knockdown of circCYFIP2 significantly enhanced or reduced the invasive abilities of HCC cells. Specifically, we also showed mechanistically that circCYFIP2 promotes the progression of GC by acted as the sponge of miR-1205. Due to the stable loop structure and high abundance in the cytoplasm,

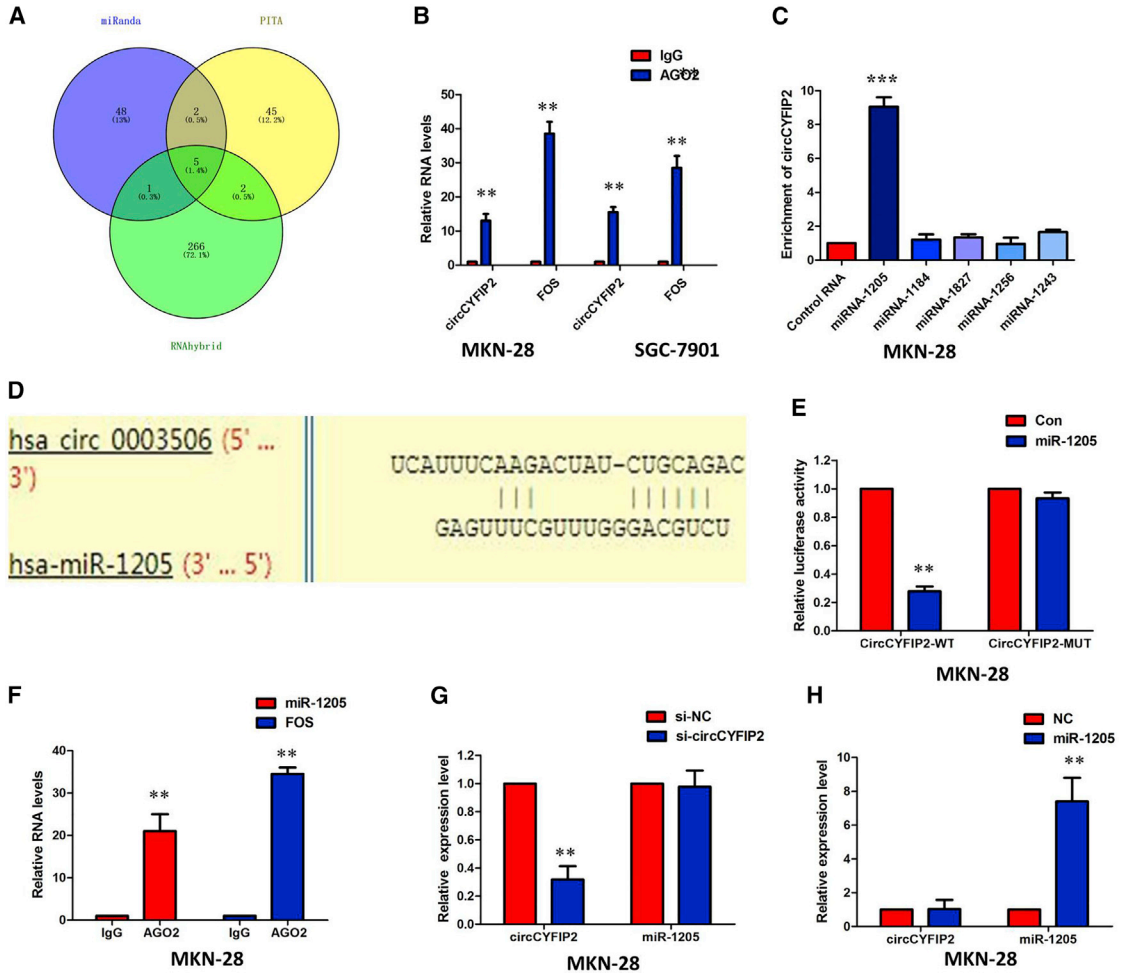

Figure 5. circCYFIP2 Acted as a miR-1205 Sponge in GC cells

(A) Schematic illustration showing the overlap of the target miRNAs of circCYFIP2 predicted by miRanda, PITA, and RNAhybrid. (B) Endogenous circCYFIP2 was efficiently pulled down by anti-Ago2. (C) miRNA pull-down assay showed that circCYFIP2 was only efficiently enriched by miR-1205. (D) The binding sequence between miR-1205 and circCYFIP2. (E) The luciferase reporter systems showed that miR-1205 mimic considerably reduced the luciferase activity of the WT-circCYFIP2 luciferase reporter vector compared with negative control, while miR-1205 mimic did not pose any impact on the luciferase activity of MUT-circCYFIP2-transfected MKN-28 cells. (F) circCYFIP2 and miR-1205 simultaneously existed in the production precipitated by anti-AGO2. (G). Silencing of circCYFIP2 did not affect the expression of miR-1205. (H) Transfection of miR-1205 mimics did not affect the expression of circCYFIP2; all tests were at least performed three times. Data were expressed as mean ± SD. **$p < 0.01$.

circCYFIP2 may be an efficient diagnostic and therapeutic target and a promising biomarker for prognosis in GC.

First, one of the major findings of the present study is that a novel up-regulated circRNA, circCYFIP2, was identified in circRNA microarray analysis from 5 GC tissues with metastasis. Moreover, elevated expression of circCYFIP2 was positively correlated with UICC stages, pathological T stages, lymphatic metastasis, distant metastasis, and grades. Kaplan-Meier survival analysis demonstrated shorter OS in GC patients with high expression of circCYFIP2. ROC curves also suggested that the validated circCYFIP2 can serve as biomarkers for diagnosing GC.

Other than functioning as potential prognosis biomarkers for GC, circRNAs have also been shown to be associated with the carcinogenesis and aggressive behavior of GC.[9,10] Here, *in vitro* functional assays revealed that gain-of-function experiments revealed that ectopic expression of circCYFIP2 promoted proliferation and inhibited apoptosis of GC cells. Loss-of-function experiments revealed that knockdown of circCYFIP2 inhibited proliferation and promoted apoptosis of GC cells. In addition, xenograft experiments showed that circCYFIP2 promoted GC xenograft growth *in vivo*. Moreover, our results showed that circCYFIP2 could significantly promote GC cell invasion ability *in vitro*, suggesting that circCYFIP2 might be a potential novel target for GC therapy.

Recently, increasing evidence has shown that circRNAs function as a sponge for miRNAs to affect tumorous biological process.[11–13] It has recently been reported that circRNAs can act as miRNA sponges to negatively control miRNA.[14] The majority of circRNAs can function

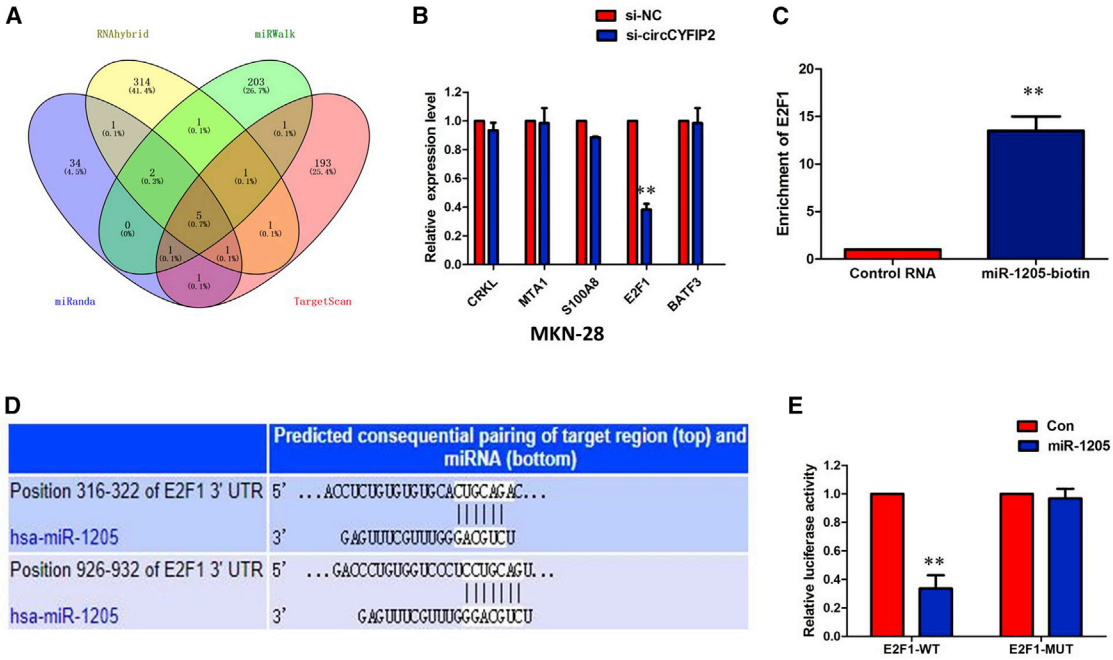

Figure 6. E2F1 Was Positively Regulated by circCYFIP2/miR-1205

(A) Venn diagram showing 5 genes that are putative miR-1205 targets computationally predicted by four algorithms (miRanda, RNAhybrid, miRWalk, and TargetScan). (B) mRNA levels of 5 candidate target genes were detected after silencing circCYFIP2. (C) miR-1205 could significantly enrich the 3′ UTR of E2F1 mRNA. (D) The binding sequence between miR-1205 and E2F1. (E) Luciferase reporter assay demonstrated miR-1205 mimics significantly decreased the luciferase activity of E2F1-WT in HCC cells. All tests were at least performed three times. Data were expressed as mean ± SD. **$p < 0.01$.

as sponges, via a mechanism of back-splicing, as they are enriched in miRNA binding sites.[15] They can also competitively bind to miRNAs and decrease the activity of miRNAs.[16] Our results further showed that circRNAs can serve as competitive endogenous RNAs and play an important role in GC development. Herein, using various assays, we found that circCYFIP2 promoted GC progression, mainly through interaction with miR-1205. Next, we verified that circFMN2 had an endogenous sponge-like effect on miR-1205 in GC. Furthermore, bioinformatics prediction and a luciferase reporter assay showed that circCYFIP2 and the E2F1 3′ UTR share identical miR-1205 response elements and might therefore bind competitively to miR-1205. Third, circCYFIP2 could bind directly to miR-1205 in an AGO2-dependent manner. Finally, circCYFIP2 regulates E2F1 expression by sponging miR-1205 because miR-1205 inhibition releases the inhibitory effect of circCYFIP2 deficiency on E2F1 expression.

miRNAs are a class of non-coding small RNAs of about 19–23 nucleotides in length, which are widely involved in various biological behaviors of cancer cells.[17] miRNAs can post-transcriptionally reduce the levels of specific target protein coding gene expression by binding to the 3′ UTR of target mRNAs and resulting in translation inhibition or mRNA degradation.[18] Studies showed that miRNAs were closely related to cell biological processes of GC.[19] Recently, miR-1205 has been reported as a tumor suppressor that is significantly downregulated in multiple cancer types.[20,21] In our study, E2F1 was predicted as the candidate target gene of miR-1205 by miRDB and Targetscan and was further testified by dual-luciferase reporter assay. Recently, a few studies have implicated that overexpression of E2F1 accelerates formation of various tumors.[22,23] We found that E2F1 was upregulated in GC according to The Cancer Genome Atlas database (http://www.targe_tscan.org/vert_71/). However, high E2F1 expression in GC tissues is not significantly associated with worse OS and worse DFS.

In conclusion, our study reveals that circCYFIP2 is upregulated in GC tissues and that high circCYFIP2 expression is correlated with tumor metastasis and unfavorable prognosis of GC patients. Moreover, enhanced circCYFIP2 expression promoted GC cell growth and motility through sponging miR-1205 to upregulate E2F1. Consequently, circCYFIP2 may have considerable potential as a prognostic predictor and therapeutic target for GC. Our findings might provide new insight into GC development and provided a novel potential strategy for GC treatment.

MATERIALS AND METHODS

Tissue Collection

The trial was approved by the Research Ethics Committee of The First Affiliated Hospital of Shantou University Medical College, and written consent was obtained from all patients. 5 GC tissues with metastasis and 5 GC tissues without metastasis were used for microarray analysis. Furthermore, 68 paired GC samples were used for the validation of microarray analysis. All samples were collected from The First Affiliated Hospital of Shantou University Medical College, between January

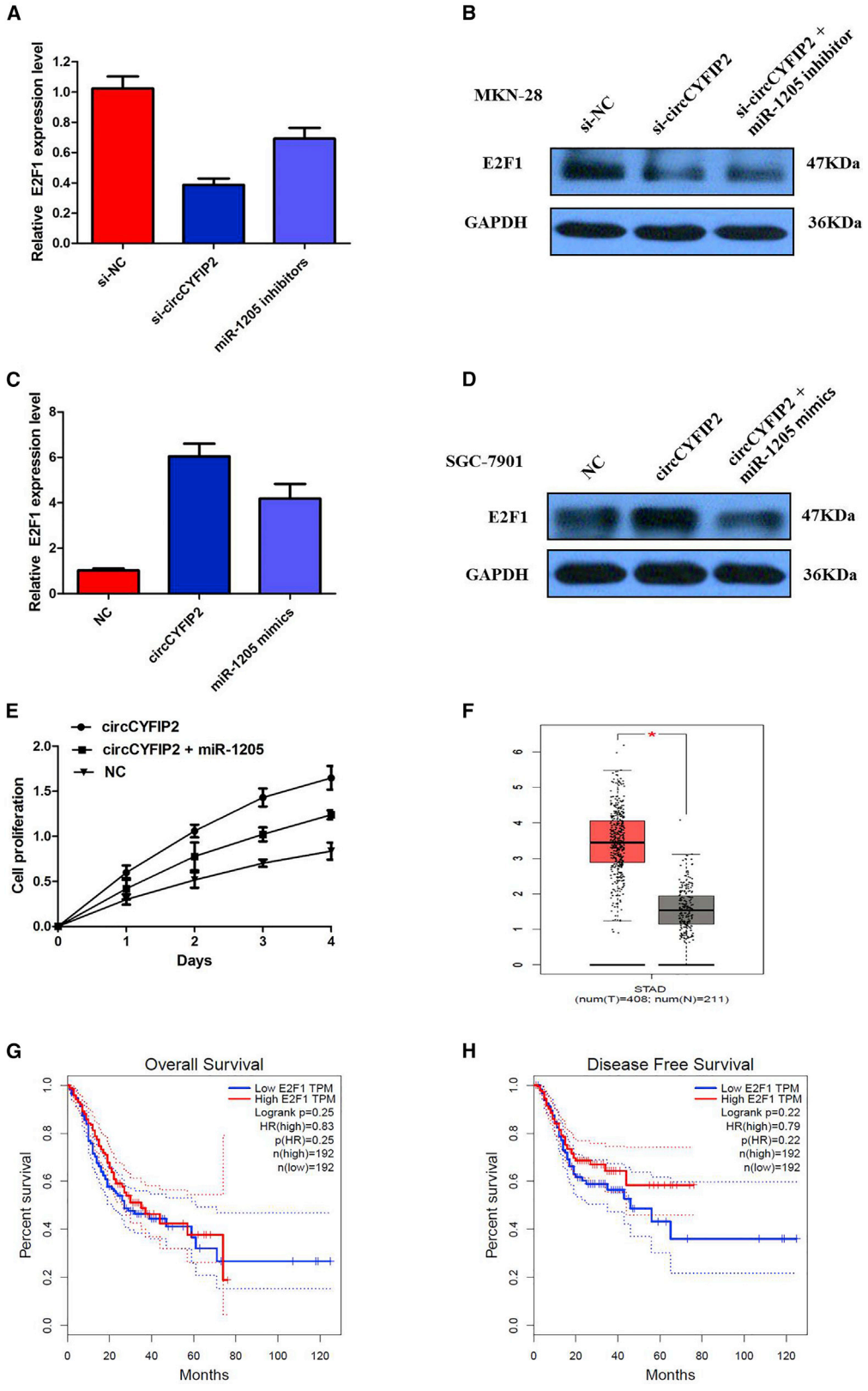

(legend on next page)

2016 and December 2018. All tissues were histologically identified, diagnosed as gastric adenocarcinoma, and graded according to the guidelines of modified American Joint Committee on Cancer (AJCC).

Cell Lines

The normal gastric mucosa epithelial GES-1 cell line and human GC cell lines (MKN-28, AGS, MKN-45, BGC-823, MGC-803, HGC-27, SGC-7901) were purchased from the Type Culture Collection of the Chinese Academy of Sciences (Shanghai, China). The cell lines were cultured in RPMI 1640 medium (Gibco, USA) containing with 10% fetal bovine serum (FBS; Gibco, USA), 100 U/mL penicillin, and 100 mg/mL streptomycin at 37°C.

Microarray Analysis

Samples (5 GC tissues with metastasis and 5 GC tissues without metastasis) were immediately frozen in liquid nitrogen after being obtained from surgical specimens. The sample preparation and microarray hybridization were performed based on the Arraystar's standard protocols (Rockville, MD, USA). After being digested with RNase R (Epicenter Technologies, Madison, WI, USA) to remove linear RNAs, circRNAs were amplified and transcribed into fluorescent circRNA utilizing Arraystar Super RNA Labeling Kit (Arraystar). Subsequently, the labeled circRNAs were hybridized onto the Arraystar Human circRNA Array (8 × 15 K, Arraystar), and then scanned by the Agilent Scanner G2505C (Jamul, CA, USA). circRNAs showing fold changes ≥ 2 and p values <0.05 were regarded as significantly differentially expressed.

Bioinformatic Analysis

Agilent Feature Extraction software (version 11.0.1.1) was used to analyze acquired array images. Data processing were performed using the R software package. Differentially expressed circRNAs with statistical significance between two groups were identified through Volcano Plot filtering. Differentially expressed circRNAs between two samples were identified through Fold Change filtering. The circRNA/miRNA interaction was predicted with Arraystar's homemade software based on miRanda, PITA, and RNAhybrid.

RNA Extraction and Quantitative Real-Time PCR

Total RNAs from cells and tissues were extracted using Trizol (Invitrogen, Carlsbad, CA, USA). Total RNAs from plasma were extracted using TRIzol LS Reagent (Invitrogen, Carlsbad, CA, USA). The RNA extraction was performed according to the manufacturer's instructions. For circRNA and mRNA, PrimeScript RT reagent Kit (Takara, Dalian, China) was used to generate cDNA; TB GreenPremix Ex Taq II (Takara, Dalian, China) was used to perform real-time PCR; 18S rRNA was utilized as internal control. For miRNA, miRcute Plus miRNA First-Strand cDNA Kit (TIANGEN, Beijing, China) was used to generate cDNA; miRcute Plus miRNA qPCR Kit (SYBR Green) was used to perform real-time PCR; U6 small nuclear RNA (snRNA) was utilized as internal control. Real-time PCR was performed using an ABI 7500 real-time PCR system (Applied Biosystems, Foster City, CA, USA). $2^{-\Delta\Delta Ct}$ method was used to calculate the relative expression of RNAs. The primers used in this study were synthesized by Sangon Biotech (Shanghai, China). The reverse primer for miRNA was supplied by the miRcute Plus miRNA qPCR Kit (SYBR Green).

TCGA Dataset Analysis

The data and the corresponding clinical information of patients were collected from TCGA database (http://cancergenome.nih.gov/). We used the edgeR package of R packages to perform the difference analysis (http://www.bioconductor.org/packages/release/bioc/html/edgeR.html) and used the pheatmap package of R packages to perform the cluster analysis (https://cran.r-project.org/web/packages/pheatmap/index.html). Sva R package was used to remove the batch effect. Genes with adjusted p values <0.05 and absolute fold changes (FCs) >1.5 were considered differentially expressed genes. Kaplan-Meier survival curves were drawn to analyze the relationships between genes and overall survival in the survival package. The corresponding statistical analysis and graphics were performed in R software (R version 3.3.2).

Plasmid, siRNAs, and miRNA Mimic, Inhibitor, Transient Transfection, and Construction of Stable Cell Lines

Plasmid-mediated circRNA overexpression and knockdown vector were obtained from Oebiotech (Shanghai, China), siRNAs targeting circRNA were obtained from GenePharma (Suzhou, China), miR-1205 mimic was ordered from RiboBio (Guangzhou, China), and the lentiviral expression vector of miR-1205 inhibitor and control plasmid were ordered from GeneCopoeia (Rockville, MD, USA). Cells were seeded in 6-well plates 24 h prior to miR-1205 mimic or inhibitor transfection with 50%–60% confluence and then were transfected with Lipofectamine 2000 (Invitrogen, Carlsbad, CA, USA) following the manufacturer's protocol. For stable transfections, we first established circRNA-0003506 and negative vector stable expressing cells using Puromycin selection methods.

Actinomycin D and RNase R Treatment

To block transcription, we added 2 mg/mL Actinomycin D or dimethyl sulfoxide (Sigma-Aldrich, St. Louis, MO, USA) as a negative control into the cell culture medium. For RNase R treatment, total RNA (2 μg) was incubated for 30 min at 37°C with or without 3 U/μg of RNase R (Epicenter Technologies, Madison, WI, USA).

Figure 7. circCYFIP2 Promotes Cell Proliferation via the circCYFIP2-miR- 1205-E2F1 Axis

(A) Inhibition of circCYFIP2 decreased of E2F1 mRNA expression was significantly recuperated following miR-1205 inhibitors. (B) Inhibition of circCYFIP2 decreased of E2F1 protein expression was significantly recuperated following miR-1205 inhibitors. (C) Overexpressing circCYFIP2 increased of E2F1 mRNA expression was significantly recuperated following miR-1205 mimics. (D) Overexpressing circCYFIP2 increased of E2F1 protein expression was significantly recuperated following miR-1205 mimics. (E) The miR-1205 mimics could partially rescue the proliferation-promoting effect induced by circCYFIP2. (F) The TCGA database showed that the level of E2F1was significantly upregulated in GC tissue compared with normal tissue. (G) Kaplan-Meier survival analysis from TCGA HCC datasets suggested that high E2F1 expression in GC tissues is not significantly associated with worse overall survival (OS). (H) Kaplan-Meier survival analysis from TCGA HCC datasets suggested that high E2F1 expression in GC tissues is not significantly associated with worse disease-free survival (DFS); all tests were at least performed three times. Data were expressed as mean ± SD. **p < 0.01.

After treatment with Actinomycin D and RNase R, quantitative real-time PCR was performed to determine the expression levels of circCYFIP2 and CYFIP2 mRNA.

Isolating RNAs from Nucleus and Cytoplasmic Fractions

The nuclear and cytoplasmic fractions were isolated using PARIS Kit (Invitrogen, Carlsbad, CA, USA) following the manufacturer's protocol. Briefly, cells were collected and lysed with cell fractionation buffer, followed by centrifugation to separate the nuclear and cytoplasmic fractions. The supernatant containing the cytoplasmic fraction was collected and transferred to a fresh RNase-free tube. The nuclear pellet was lysed with Cell Disruption Buffer. The cytoplasmic fraction and nuclear lysate were mixed with 2X Lysis/Binding Solution and then added with 100% ethanol. The sample mixture was drawn through a Filter Cartridge, followed by washing with Wash Solution. The RNAs of nuclear and cytoplasmic fractions were eluted with Elution Solution. U6 snRNA and GAPDH were employed as positive control for nuclear and cytoplasmic fractions, respectively.

CCK-8 Assay

Each group of cells in logarithmic phase was prepared into a single--cell suspension, and the cell density adjusted at 1,000 cells per well were seeded in a 96-well plate. Following that, six replicate wells were set in each group. On the second day, after the cells were attached, 10 μL of CCK-8 solution (Beyotime Biotechnology) was added to the sample, and a blank control well only containing the medium and CCK-8 solution was set. After incubating for 1 h, a microplate reader at a wavelength of 450 nm was employed to determine and record the absorbance (OD) values of each well. Ultimately, the plate was measured at intervals of 24 h for 5 days.

Cell Apoptosis Flow Cytometry Analyses

At 48 h after transfection, transfected cells were harvested by trypsinization and resuspended in cold phosphate-buffered saline for analysis. The rate of cell apoptosis was detected using an Annexin V-fluorescein isothiocyanate (FITC)/propidium iodide (PI) apoptosis detection kit (BD Biosciences, San Jose, CA, USA) according to the manufacturer's instructions.

Cell Wound Healing and Transwell Assays

For cell wound healing assay, the cells were first cultured to full confluence in 6-well plates. Subsequently, the cells were scratched with a 200 μL micropipette tip in the center of the well. Then, the cells were incubated with serum-free medium. Representative images were captured at 0 h and 24 h after injury. The width of wound healing was quantified and compared with baseline values. All experiments were repeated independently in triplicate.

Transwell experiment was carried out using transwell chamber (Millipore, Billerica, USA). In the migration assay, the transfected GC cells were centrifuged at 1,000 r/min for 3 min after trypsinization, and the cells were resuspended in serum-free medium and the density was adjusted to 1×10^5/mL. Then, 200 μL of the cell suspension was added to the upper compartment of the transwell chamber. In all, 700 μL of medium containing 10% FBS was added to the lower compartment. Then the cells were cultured for 24 h. Ultimately, the chamber was removed and the cells on the upper compartment were gently wiped with a cotton swab. Then, the cells passing through the membrane were fixed and stained with crystal violet solution for 30 min and washed twice with PBS. After they were dried, the cells were observed with a microscope, and five fields of view (×100) were randomly selected for counting. The mean value was considered as the number of migrated cells. In invasion assay, 50 μL Matrigel was diluted and coated on the upper compartment, and other experimental procedures were the same as the migration experiment.

Animal Experiments

To establish xenograft mouse models, we cloned the small hairpin RNA (shRNA) against circCYFIP2 (the same target with si-circ-1) and negative control into pLL3.7 vector, and we cloned the full-length cDNA of circCYFIP2 or a negative control into PLCDH-ciR vector, containing a front and back circular frame. Then, the stable cell lines with knockdown or overexpression of circCYFIP2 were constructed with MKN-28 or SGC-7901 cells. For *in vivo* tumorigenesis assay, 1.0×10^7 MKN-28 or SGC-7901 cells in 150 μL PBS were subcutaneously injected into left inguinal region of male BALB/c athymic nude mice (4 weeks old). Tumor volumes were calculated by the formula: tumor = (length × width2)/2 and measured every 4 days. Finally, the mice were sacrificed, and the volume and weight of tumors were detected. The animal experiments complied strictly with the Animal Care guidelines of The First Affiliate Hospital, School of Medicine, Shantou University.

Immunohistochemistry

The expression of Ki67 in tumor tissues from nude mice was analyzed by immunohistochemical analysis. Briefly, the tissues were fixed with 4% formaldehyde for 24 h, embedded, and cut into 4-μm-thick section. The sections were treated with 10 mmol/L sodium citrate buffer and incubated with anti-Ki67 antibody (1:200 dilution) overnight at 4°C. The positive signaling was stained by using a mouse- and rabbit-specific horseradish peroxidase (HRP)/DAB (ABC) Detection IHC kit (Abcam Trading [Shanghai] Company, Shanghai, China), and counterstained with hematoxylin. The relative integral optical density (IOD) of positive signaling was obtained by ImageJ software.

RIP Assay

RIP assay was performed using an EZ-Magna RiP Kit (Millipore, Billerica, MA, USA) in accordance with the manufacturer's instructions. Cells were lysed at 70%–80% confluence in RIP lysis buffer, and then incubated with magnetic beads conjugated with human anti-Ago2 antibody (Millipore) and normal mouse IgG control (Millipore) in RIP buffer. The RNAs in the immunoprecipitates were isolated with Trizol reagent and analyzed by quantitative real-time PCR.

Luciferase Reporter Assay

The sequence of circRNA containing the putative or mutated putative binding sites for miR-1205 was cloned into pmirGLO vector (Promega, Madison, WI, USA). PmirGLO-circCYFIP2-WT reporter and pmirGLO-circCYFIP2-MUT reporter were co-transfected into

cells with miR-1205 mimics and miR-NC. Lipofectamine 2000 was used for transfection. 48 h after transfection, luciferase reporter assay was performed using the dual-luciferase reporter assay system (Promega). The luciferase activity was normalized to Renilla luciferase activity.

Western Blot Analysis

For western blot analysis, cells were extracted using a protein extraction kit (Key Gene, KGP9100). Lipid proteins were added into 8%, 10%, 12%, or 15% gels, subjected to 120 V to promote migration, and then transferred onto nitrocellulose membranes. The membranes were blocked with 5% BSA in TBST buffer and incubated with specific primary antibodies at 4°C overnight. The primary antibodies against E2F1 were obtained from Cell Signaling Technology (CST, Beverly, MA, USA). The next day, membranes were washed 3 times for 15 min in TBST and incubated with secondary antibodies for 2 h at room temperature. HRP substrate (WBKL0100, Millipore, USA) was used to detect the protein bands (Molecular Imager, ChemiDoc XRS+, Bio-Rad, USA), and the band intensities were quantified using Image-Pro Plus software (Mediacy, USA).

Statistical Analysis

Data were analyzed in GraphPad Prism software (GraphPad Software, La Jolla, CA, USA). Overall survival analysis was performed by Kaplan-Meier curves and log-rank test for significance. Student's t test with two tails was used to assess the statistical significance in two groups and one-way ANOVA with post hoc Bonferroni test were used in three or more groups. Correlations were analyzed by Pearson correlation test. $p < 0.05$ was considered statistically significant.

SUPPLEMENTAL INFORMATION

Supplemental Information can be found online at https://doi.org/10.1016/j.omtn.2020.05.007.

AUTHOR CONTRIBUTIONS

J.L. performed primers design and experiments. S.L. and E.L. contributed cell and animal experiments. Z.L. and R.Z. collected and classified the human tissue samples. X.W. analyzed the data. W.Z. wrote the paper. All authors read and approved the final manuscript.

CONFLICTS OF INTEREST

The authors declare no competing interests.

ACKNOWLEDGMENTS

The datasets supporting the conclusions of this article are included within the article and Supplemental Information. Shantou Medical and Health Technology Project (No.180418184011332).

REFERENCES

1. Bray, F., Ferlay, J., Soerjomataram, I., Siegel, R.L., Torre, L.A., and Jemal, A. (2018). Global cancer statistics 2018: GLOBOCAN estimates of incidence and mortality worldwide for 36 cancers in 185 countries. CA Cancer J. Clin. *68*, 394–424.

2. Ferlay, J., Soerjomataram, I., Dikshit, R., Eser, S., Mathers, C., Rebelo, M., Parkin, D.M., Forman, D., and Bray, F. (2015). Cancer incidence and mortality worldwide: sources, methods and major patterns in GLOBOCAN 2012. Int. J. Cancer *136*, E359–E386.

3. Zhao, T.T., Xu, H., Xu, H.M., Wang, Z.N., Xu, Y.Y., Song, Y.X., Yin, S.C., Liu, X.Y., and Miao, Z.F. (2018). The efficacy and safety of targeted therapy with or without chemotherapy in advanced gastric cancer treatment: a network meta-analysis of well-designed randomized controlled trials. Gastric Cancer *21*, 361–371.

4. Qu, S., Yang, X., Li, X., Wang, J., Gao, Y., Shang, R., Sun, W., Dou, K., and Li, H. (2015). Circular RNA: A new star of noncoding RNAs. Cancer Lett. *365*, 141–148.

5. Memczak, S., Papavasileiou, P., Peters, O., and Rajewsky, N. (2015). Identification and characterization of circular RNAs as a new class of putative biomarkers in human blood. PLoS ONE *10*, e0141214.

6. Shang, Q., Yang, Z., Jia, R., and Ge, S. (2019). The novel roles of circRNAs in human cancer. Mol. Cancer *18*, 6.

7. Salzman, J., Chen, R.E., Olsen, M.N., Wang, P.L., and Brown, P.O. (2013). Cell-type specific features of circular RNA expression. PLoS Genet. *9*, e1003777.

8. Vo, J.N., Cieslik, M., Zhang, Y., Shukla, S., Xiao, L., Zhang, Y., Wu, Y.M., Dhanasekaran, S.M., Engelke, C.G., Cao, X., et al. (2019). The landscape of circular RNA in Cancer. Cell *176*, 869–881.

9. Wang, N., Lu, K., Qu, H., Wang, H., Chen, Y., Shan, T., Ge, X., Wei, Y., Zhou, P., and Xia, J. (2020). CircRBM33 regulates IL-6 to promote gastric cancer progression through targeting miR-149. Biomed. Pharmacother. *125*, 109876.

10. Deng, G., Mou, T., He, J., Chen, D., Lv, D., Liu, H., Yu, J., Wang, S., and Li, G. (2020). Circular RNA circRHOBTB3 acts as a sponge for miR-654-3p inhibiting gastric cancer growth. J. Exp. Clin. Cancer Res. *39*, 1.

11. Song, J., Wang, H.L., Song, K.H., Ding, Z.W., Wang, H.L., Ma, X.S., Lu, F.Z., Xia, X.L., Wang, Y.W., Fei-Zou, and Jiang, J.Y. (2018). CircularRNA_104670 plays a critical role in intervertebral disc degeneration by functioning as a ceRNA. Exp. Mol. Med. *50*, 94.

12. Su, H., Tao, T., Yang, Z., Kang, X., Zhang, X., Kang, D., Wu, S., and Li, C. (2019). Circular RNA cTFRC acts as the sponge of MicroRNA-107 to promote bladder carcinoma progression. Mol. Cancer *18*, 27.

13. Yang, R., Xing, L., Zheng, X., Sun, Y., Wang, X., and Chen, J. (2019). The circRNA circAGFG1 acts as a sponge of miR-195-5p to promote triple-negative breast cancer progression through regulating CCNE1 expression. Mol. Cancer *18*, 4.

14. Ruan, Y., Li, Z., Shen, Y., Li, T., Zhang, H., and Guo, J. (2020). Functions of circular RNAs and their potential applications in gastric cancer. Expert Rev. Gastroenterol. Hepatol. *14*, 85–92.

15. Tang, X., Zhu, J., Liu, Y., Chen, C., Liu, T., and Liu, J. (2019). Current Understanding of Circular RNAs in Gastric Cancer. Cancer Manag. Res. *11*, 10509–10521.

16. Lu, J., Wang, Y.H., Yoon, C., Huang, X.Y., Xu, Y., Xie, J.W., Wang, J.B., Lin, J.X., Chen, Q.Y., Cao, L.L., et al. (2020). Circular RNA circ-RanGAP1 regulates VEGFA expression by targeting miR-877-3p to facilitate gastric cancer invasion and metastasis. Cancer Lett. *471*, 38–48.

17. Ambros, V. (2004). The functions of animal microRNAs. Nature *431*, 350–355.

18. Nishibeppu, K., Komatsu, S., Imamura, T., Kiuchi, J., Kishimoto, T., Arita, T., Kosuga, T., Konishi, H., Kubota, T., Shiozaki, A., et al. (2020). Plasma microRNA profiles: identification of miR-1229-3p as a novel chemoresistant and prognostic biomarker in gastric cancer. Sci. Rep. *10*, 3161.

19. Ohzawa, H., Kumagai, Y., Yamaguchi, H., Miyato, H., Sakuma, Y., Horie, H., Hosoya, Y., Kawarai Lefor, A., Sata, N., and Kitayama, J. (2019). Exosomal microRNA in peritoneal fluid as a biomarker of peritoneal metastases from gastric cancer. Ann. Gastroenterol. Surg. *4*, 84–93.

20. Li, P., Lin, X.J., Yang, Y., Yang, A.K., Di, J.M., Jiang, Q.W., Huang, J.R., Yuan, M.L., Xing, Z.H., Wei, M.N., et al. (2019). Reciprocal regulation of miR-1205 and E2F1 modulates progression of laryngeal squamous cell carcinoma. Cell Death Dis. *10*, 916.

21. Yan, H., Chen, X., Li, Y., Fan, L., Tai, Y., Zhou, Y., Chen, Y., Qi, X., Huang, R., and Ren, J. (2019). MiR-1205 functions as a tumor suppressor by disconnecting the synergy between KRAS and MDM4/E2F1 in non-small cell lung cancer. Am. J. Cancer Res. *9*, 312–329.

22. Endo, M., Tanaka, Y., Otsuka, M., and Minami, Y. (2020). E2F1-Ror2 signaling mediates coordinated transcriptional regulation to promote G1/S phase transition in bFGF-stimulated NIH/3T3 fibroblasts. FASEB J. *34*, 3413–3428.

23. Zhao, M., Liu, Y., Chang, J., Qi, J., Liu, R., Hou, Y., Wang, Y., Zhang, X., Qiao, L., and Ren, L. (2019). ILF2 cooperates with E2F1 to maintain mitochondrial homeostasis and promote small cell lung cancer progression. Cancer Biol. Med. *16*, 771–783.